We are IntechOpen, the world's leading publisher of Open Access books Built by scientists, for scientists

4,800
Open access books available

122,000
International authors and editors

135M
Downloads

Our authors are among the

154
Countries delivered to

TOP 1%
most cited scientists

12.2%
Contributors from top 500 universities

WEB OF SCIENCE™

Selection of our books indexed in the Book Citation Index in Web of Science™ Core Collection (BKCI)

Interested in publishing with us?
Contact book.department@intechopen.com

Numbers displayed above are based on latest data collected.
For more information visit www.intechopen.com

1

Supervisory Control for Turnover Prevention of a Teleoperated Mobile Agent with a Terrain-Prediction Sensor Module

Jae Byung Park & Beom Hee Lee
Seoul National University
Seoul, Korea

1. Introduction

Teleoperated mobile agents (or vehicles) play an important role especially in hazardous environments such as inspecting underwater structures (Lin, 1997), demining (Smith, 1992), and cleaning nuclear plants (Kim, 2002). A teleoperated agent is, in principle, maneuvered by an operator at a remote site, but should be able to react autonomously to avoid dangerous situations such as collisions with obstacles and turnovers. Many studies have been conducted on collision avoidance of mobile agents (Borenstein, 1989; Borenstein, 1991a; Borenstein, 1991b; Howard, 2001; Niwa, 2004; Singh et al., 2000). In this research, however, we will focus on turnover prevention of mobile agents moving on uneven terrain because a turnover can cause more fatal damage to the agents. Here, we adopt the term 'turnover' as a concept which includes not only a rollover but also a pitchover.

Extensive studies have been conducted on motion planning problems of mobile agents traveling over sloped terrain in the robotics research community (Shiller, 1991). Shiller presented optimal motion planning for an autonomous car-like vehicle without a slip and a rollover. The terrain was represented by a *B*-spline patch and the vehicle path was represented by a *B*-spline curve, where the terrain and vehicle path were given in advance. With the models of the terrain and the path, the translational velocity limit of the vehicle was determined to avoid a slip and a rollover. Also, many studies have been conducted on rollover prevention of heavy vehicles like trucks and sports utility vehicles in the vehicular research community. Takano analyzed various dynamic outputs of large vehicles, such as the lateral acceleration, yaw rate, roll angle, and roll rate, in the frequency domain for predicting rollovers (Takano, 2001). Chen developed the time-to-rollover (TTR)-based rollover threat index in order to predict rollovers of sports utility vehicles (Chen, 1999). This intuitive measure TTR was computed from the simple model and then corrected by using an artificial neural network. Nalecz et al. suggested an energy-based function called the rollover prevention energy reserve (RPER) (Nalecz, 1987; Nalecz, 1991; Nalecz, 1993). RPER is the difference between the energy needed to bring the vehicle to its rollover position and the rotational kinetic energy, which can be transferred into the gravitational potential energy to lift the vehicle. RPER is positive for

Source: Mobile Robots, Moving Intelligence, ISBN: 3-86611-284-X, Edited by Jonas Buchli, pp. 576, ARS/plV, Germany, December 2006

non-rollover cases and negative for rollover cases. Acarman analyzed the rollover of commercial vehicles with tanks that are partially filled with liquid cargo (Acarman, 2003). In this case, the frequency shaped backstepping sliding mode control algorithm was designed to stabilize and attenuate the sloshing effects of the moving cargo by properly choosing the crossover frequencies of the dynamic compensators in accordance with the fundamental frequencies of the slosh dynamics.

Many studies have been conducted on turnover prevention of mobile manipulators like a fork lift. Rey described the scheme for automatic turnover prediction and prevention for a forklift (Rey, 1997). By monitoring the static and dynamic turnover stability margins of a mobile manipulator, it is possible to predict turnovers and take appropriate actions to prevent turnovers. Here, the dynamic force-angle measure of turnover stability margin proposed by Papadopoulos (Papadopoulos, 1996) is employed. Also, Sugano suggested the concepts about stability such as the stability degree and the valid stable region based on the zero-moment point (ZMP) criterion to evaluate the stability for a mobile manipulator (Sugano, 1993). In addition, the method of ZMP path planning with a stability potential field was suggested for recovering and maintaining stability (Huang, 1994). Based on the path planning method, the motion of the manipulator is planned in advance to ensure stability while the vehicle is in motion along a given trajectory. Furthermore, for stability recovery, the compensation motion of the manipulator is derived by using the redundancy of the manipulator, taking into consideration the manipulator configuration and the static system stability (Huang, 1997).

In the abovementioned researches for an autonomous mobile agent, the path and trajectory of a vehicle and a manipulator were given in advance and modified for rollover prevention. However, the path and trajectory of a teleoperated mobile agent cannot be given in advance since both of them are determined by a teleoperator at each time instant. Thus, it is impossible to analyze and prevent rollovers in advance. For a fork lift mentioned above, its path and trajectory were not known in advance since it was maneuvered by an operator. Thus, the previous researchers estimated the path and trajectory using the proprioceptive sensor data (internal sensor data) for turnover prevention. However, in the case where there is a potential risk of turnovers due to an abrupt change in the configuration of the ground, the proprioceptive sensor data is not enough to prevent turnovers. Therefore, in this research, a low-cost terrain-prediction sensor with a camera vision and a structured laser light is proposed for predicting turnovers at front terrain before the agent arrives there. With these predicted data, a turnover prevention algorithm is suggested with the quasi-static rollover analysis of a rigid vehicle (Gillespie, 1992).

A proposed turnover prevention algorithm (Park, 2006a) consists of a pitchover prevention algorithm and a rollover prevention algorithm (Park, 2006b). According to the turnover prevention algorithm, the translational and rotational velocities of the agent are restricted for avoiding turnovers. However, the turnover prevention control brings about some inconsistencies between the intended motion and the reactive motion of the agent. For compensating these inconsistencies, we propose a force reflection technique based on virtual reality. A force reflection technique has already been used in various research areas such as medical surgery (Chen, 1998; Basdogan, 2004; Nudehi, 2005), micromanipulation (Ando, 2001; Boukhnifer, 2004), and obstacle avoidance of teleoperated mobile agents (Park, 2003a; Park, 2003b; Park, 2004; Park, 2006b). In this research, a reflective force helps an operator

control the agent without a turnover, where a 2-DOF force-feedback joystick is used as a Haptic device which can not only receive an operator's command from an operator but also send back a reflective force to him.

2. Teleoperation System

2.1 Supervisory Control

In a teleoperation system, an operator, in principle, controls a mobile agent at a remote site using a force feedback joystick, but the agent needs to control itself autonomously for escaping dangerous situations like overturning. As a result of autonomous control, the reactive motion of the agent may be different from the intended motion of an operator. It is to violate the principle rule of a teleoperation system as mentioned above. So we analyze boundaries of safe motion of an agent without turnovers and allow an operator to freely control the agent within the analyzed safe boundaries. That is, the agent motion determined by an operator is restricted for turnover prevention only when the agent motion is beyond the safe boundaries. Thus, the resultant motion of the agent is determined by the closest motion to the intended motion of an operator among the turnover-free motions. In addition, we propose a force feedback technique for an operator to recognize the inconsistency between the reactive and intended motions of an agent. If the agent controlled by an operator is faced with danger, the operator feels reflective force generated by the force feedback joystick for preventing the operator from controlling the agent beyond the safe boundaries. Thus, reflective force makes it possible that the operator drives the agent without turnovers.

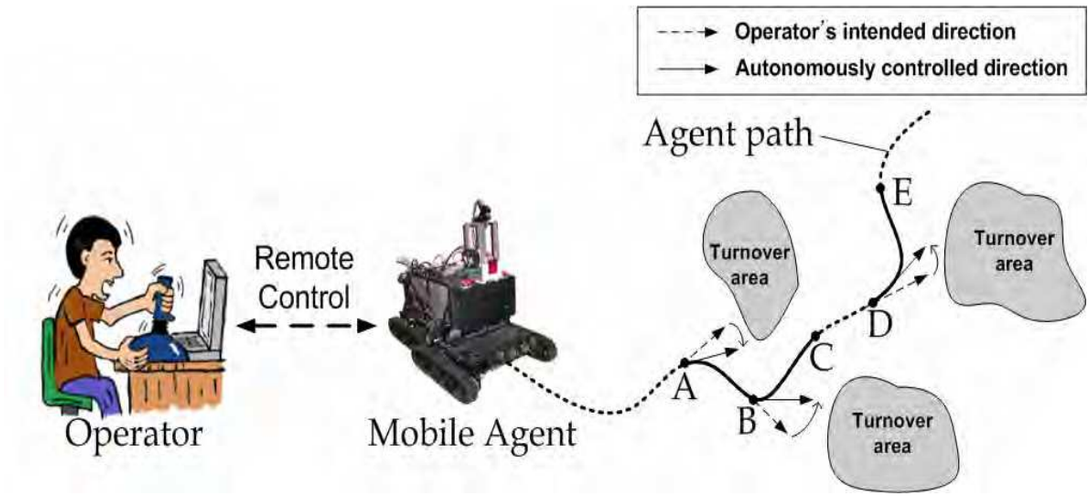

Fig. 1. Supervisory control of a teleoperation system with a mobile agent. (A-C, D-E: Autonomously controlled path segment for turnover prevention).

An example of the supervisory control is shown in Fig. 1. An agent moves to **A** according to an operator's command. From **A** to **C**, the agent is autonomously controlled for avoiding turnovers since it detects a potential turnover area. From **C**, the agent is controlled by an operator since the agent escapes from danger of turnovers. Again, the agent is autonomously controlled for turnover prevention from **D** to **E**. As described above, the operator's intended direction of the agent is modified by the autonomously controlled

direction for turnover prevention in the case that the agent detects potential turnovers. Also, whenever the agent is autonomously controlled, the operator feels reflective force and is able to recognize the modified agent motion. However, in the case that there is no danger of turnovers, the agent is controlled by an operator.

2.2 System Configuration

The teleoperation system consists of a remote control system (RCS) and a mobile agent system (MAS) as shown in Fig. 2. The RCS and the MAS communicate with each other via wireless Ethernet communication. Control signals and sensor data are denoted in Table 1. The RCS receives input force $\boldsymbol{F}_o(t)$ from an operator via a force feedback joystick, and the joystick position $\boldsymbol{P}_J(t)$ is determined by $\boldsymbol{F}_o(t)$. Then, velocity command $\boldsymbol{V}_{cmd}(t)$ of the agent is determined from $\boldsymbol{P}_J(t)$ by a position-to-velocity matcher, where $\boldsymbol{V}_{cmd}(t)$ consists of the translational velocity $v(t)$ and rotational velocity $\omega(t)$. Here, each velocity can be controlled independently since the agent used in this research is a differential-drive machine which has two individually motorized tracks. The operator's command $\boldsymbol{V}_{cmd}(t)$ is restricted by a turnover prevention controller for avoiding potential turnovers using predicted terrain data $\boldsymbol{Tr}(t)$ transmitted from the MAS. Finally, the resultant velocity command $\boldsymbol{V}_d(t)$ for turnover prevention is transmitted to the MAS for actually controlling the agent without turnovers. Also, reflective force $\boldsymbol{F}_R(t)$ is generated by $\boldsymbol{P}_{ub}(t)$ to $\boldsymbol{P}_{lb}(t)$, where $\boldsymbol{P}_{ub}(t)$ and $\boldsymbol{P}_{lb}(t)$ are determined by upper and lower bounds, $\boldsymbol{V}_{ub}(t)$ and $\boldsymbol{V}_{lb}(t)$, for turnover-free ranges of $v(t)$ and $\omega(t)$, respectively. As a result of force reflection, an operator can intuitively recognize whether the agent motion is restricted for turnover prevention or not.

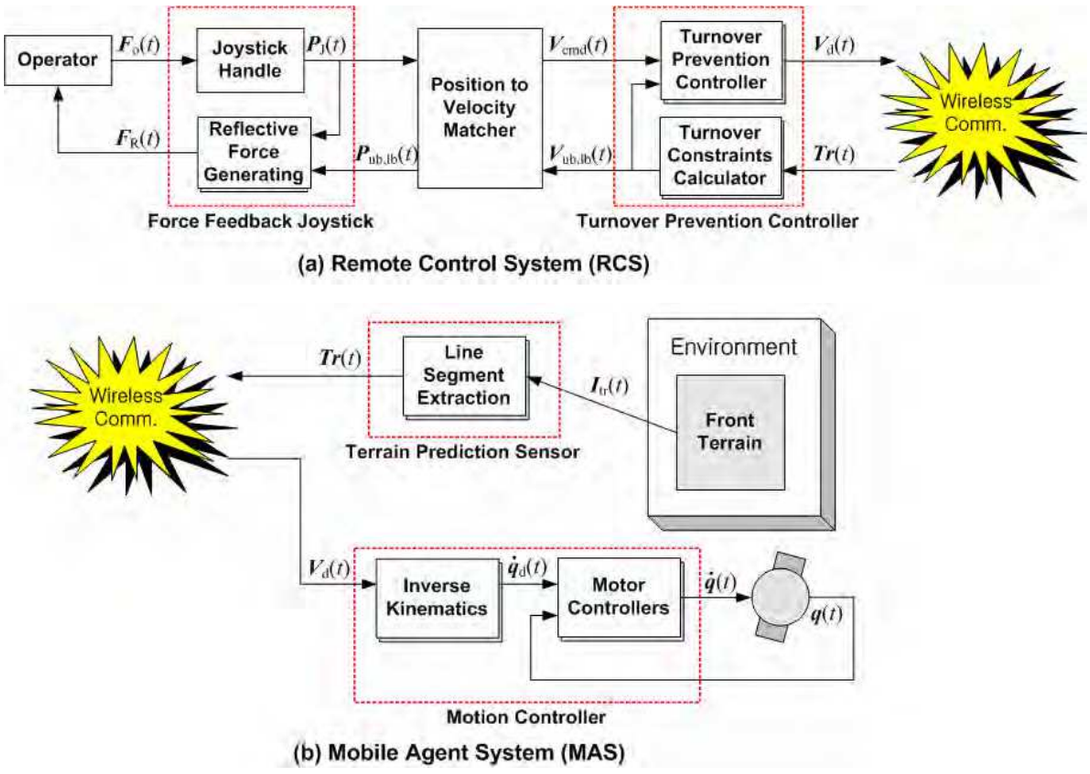

Fig. 2. Teleoperation system which is comprised of the RCS and the MAS.

Symbols	Descriptions
$\boldsymbol{F}_{\mathrm{O}}(t)$	Input force by an operator's command
$\boldsymbol{F}_{\mathrm{R}}(t)$	Reflective force generated by the force feedback joystick
$\boldsymbol{P}_{\mathrm{J}}(t)$	Joystick position determined by $\boldsymbol{F}_{\mathrm{O}}(t)$
$\boldsymbol{V}_{\mathrm{ub}}(t), \boldsymbol{V}_{\mathrm{lb}}(t)$	Upper and lower bounds of the translational and rotational velocities for avoiding turnovers
$\boldsymbol{P}_{\mathrm{ub}}(t)$, $\boldsymbol{P}_{\mathrm{lb}}(t)$	Joystick positions determined by $\boldsymbol{V}_{\mathrm{ub}}(t)$ and $\boldsymbol{V}_{\mathrm{lb}}(t)$
$\boldsymbol{V}_{\mathrm{cmd}}(t)$	Control command of the agent determined by $\boldsymbol{P}_{\mathrm{J}}(t)$
$\boldsymbol{V}_{\mathrm{d}}(t)$	Desired velocities for turnover prevention determined by $\boldsymbol{V}_{\mathrm{cmd}}(t)$, $\boldsymbol{V}_{\mathrm{ub}}(t)$ and $\boldsymbol{V}_{\mathrm{lb}}(t)$
$\boldsymbol{I}_{\mathrm{tr}}(t)$	Terrain image data obtained by the camera vision with the structured laser light
$\boldsymbol{Tr}(t)$	Terrain data obtained after image processing of $\boldsymbol{I}_{\mathrm{tr}}(t)$
$\dot{\mathbf{q}}_{\mathrm{d}}(t)$	Desired spinning speeds of the actual motors
$\dot{\mathbf{q}}(t)$	Actual spinning speeds of the motors
$\mathbf{q}(t)$	Encoder data of the motors

Table 1. Symbols of control signals and sensor data.

The MAS is composed of a mobile agent and a proposed terrain-prediction sensor module. The ROBHAZ-DT which is developed by the Korea Institute of Science and Technology (KIST) and Yujin Robotics Co., Ltd. is employed as an actual mobile agent. KIST and Yujin Robitcs Co., Ltd. are developing various ROBHAZ-series with high mobility for conducting dangerous tasks such as rescue mission, explosive ordnance disposal (EOD), mine exclusion and scout. The ROBHAZ-DT3 conducted military missions such as reconnaissance and explosive detection with Korean troops in Iraq for six months in 2004. Also, the improved model Roscue of the ROBHAZ took first, second and third prizes for rescue robots at the RoboCup 2004 in USA, the RoboCup 2005 in Japan and the RoboCup 2006 in Germany, respectively. For more information about the ROBHAZ-series, you can found at *http://www.robhaz.com*. The ROBHAZ-DT used in this research is an early prototype with double tracks as shown in Fig. 3. The MAS computes the desired spinning speeds $\dot{\mathbf{q}}_{\mathrm{d}}(t)$ of two drive wheels for the desired velocity command $\boldsymbol{V}_{\mathrm{d}}(t)$ received from the RCS, and sends them to the embedded controllers that control the actual motors to achieve the desired spinning speeds through internal feedback control loops with encoder data $\mathbf{q}(t)$. Next, front terrain data $\boldsymbol{Tr}(t)$ for turnover prevention are obtained by the terrain-prediction sensor module, which projects a structured laser light on the front terrain and detects the projected line using a web camera. In this case, the laser-line segment is extracted from terrain image data $\boldsymbol{I}_{\mathrm{tr}}(t)$ on the camera image plane for obtaining $\boldsymbol{Tr}(t)$. Finally, the obtained terrain data $\boldsymbol{Tr}(t)$ is transmitted to the RCS for turnover prevention.

Let time T_s be the communication period between the RCS and the MAS. Then time T_s should satisfy

$$T_s > T_a + 2T_d \tag{1}$$

where T_a is the maximum delay for sensor acquisition and T_d is the maximum delay for wireless communication. If the accessible range of IEEE 802.11b based Wireless Local Area Networks (WLANs) used in our system covers the locations of both RCS and MAS, the

round-trip time delay $2T_d$ (less than 0.29 ms) can be neglected as compared with time T_a (less than 100 ms). As the sum of communication packet sizes of both control signals and sensor data is less than 200 bytes (or 1600 bits) and the IEEE 802.11b standard promises data rates up to 11 Mbps, the time delay $2T_{\mathrm{d}}$ can be bounded in 0.29 ms. Although the coverage of the WLANs is reduced in crowded areas, the coverage can be easily expanded by establishing additive wireless Access Points (APs) in the areas. Also, the motion control of the agent can be completed in time T_s since the motion control time is much less than T_a and the motion control is conducted simultaneously with sensor acquisition. Hereafter, the translational velocity $v(t)$ and the rotational velocity $\omega(t)$ will be discretely described as $v(k)$ and $\omega(k)$, based on time index k which denotes time $t = kT_{\mathrm{s}}$. Of course, control signals and sensor data will also be described with k instead of t.

Fig. 3. ROBHAZ-DT (Robot for Hazardous Application-Double Track).

2.3 Basic Assumptions

Basic assumptions are introduced for terrain prediction and turnover prevention control as follows:

1. The communication period T_s between the RCS and the MAS ensures enough time to complete the terrain data acquisition and the motion control of the agent, taking into consideration the maximum time delay for wireless communication.
2. No turnover occurs between the starting position of the agent and the first detected terrain position by the terrain-prediction sensor since the agent is impossible to avoid turnovers without terrain sensor data.
3. The process for terrain data acquisition is fast enough to obtain sufficient terrain data for turnover prevention control at each time instant. At least much more than two are available within the longitudinal length of the agent while the agent moves at its normal speed.
4. The agent is represented as one lumped mass located at its center of gravity (CG) with appropriate mass and inertia properties since all components of the agent move together. The point mass at the CG, with appropriate rotational moments of inertia, is dynamically equivalent to the agent itself for all motions in which it is reasonable to assume the agent to be rigid (Gillespie, 1992).
5. The agent has a trapezoidal velocity profile. That is, the translational acceleration of the agent is determined by constant values such as a_c for accelerated motion, 0 for uniform motion and $-a_c$ for decelerated motion.

6. The motion controllers of the agent control the translational acceleration with tolerable errors according to the reference inputs such as a_c, 0 and $-a_c$. Therefore, we do not consider the variation of the acceleration depending on the various terrain types such as rocky and sandy terrain.
7. The agent is able to reduce its translational velocity from v_{max} to 0 for a distance of D_{tr}, where D_{tr} is the reference distance to the front terrain detected for turnover prevention control at each time instant. In other words, D_{tr} is defined to satisfy the condition $D_{tr} > v^2_{max}/2a_c$. Thus, taking the condition for D_{tr} into consideration, the configuration of the terrain-prediction sensor module such as the orientations of the camera and the laser-line generator should be determined. According to this assumption, even though the agent detects inevitable turnover terrain at a distance of D_{tr}, it can reduce the translational velocity and stop before arriving at the detected terrain.

3. Front Terrain Prediction

3.1 Terrain-prediction Sensor Module

We develop a low-cost terrain-prediction sensor module for obtaining front terrain data in advance. As shown in Fig. 4, the developed terrain-prediction sensor module consists of a web camera, a laser-line generator and an inclinometer, and is attached to the ROBHAZ-DT. The laser-line generator LM-6535ML6D developed by Lanics Co., Ltd. is used to project a line segment on front terrain. The fan angle and line width of the laser-line generator are 60° and 1 mm, respectively. The wavelength of the laser beam ranges from 645 nm to 665 nm and the optical output power is 25 mW. The complementary metal-oxide-semiconductor (CMOS) web camera ZECA-MV402 developed by Mtekvision Co., Ltd. is used to detect the line segment projected onto the front terrain. The inclinometer 3DM developed by MicroStrain Inc. is used to measure the absolute angles from 0° to 360° on both yaw and pitch axes, and from −70° to 70° on the roll axis with respect to the universal frame. The data of the inclinometer are obtained via RS232 Serial interface.

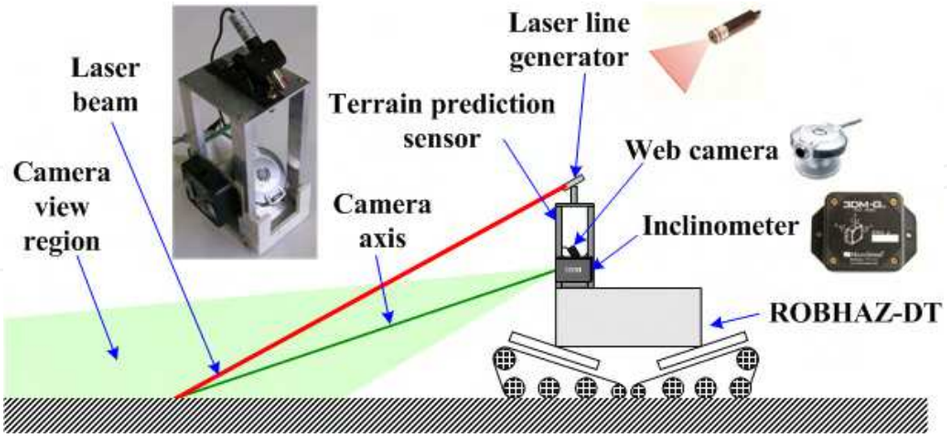

Fig. 4. Low-cost terrain prediction sensor module attached to the ROBHAZ-DT.

3.2 Acquisition of Vision Data

For terrain data acquisition, we first propose an image processing method for extracting a projected laser line from an original camera image where the image size is 320×240 pixels.

The partitioning an image into regions such as an object and the background is called segmentation (Jain, 1995). A binary image for an object and the background is obtained using an appropriate segmentation of a gray scale image. If the intensity values of an object are in an interval and the intensity values of the background pixels are outside this interval, a binary image can be obtained using a thresholding operation that sets the points in that interval to 1 and points outside that interval to 0. Thus, for binary vision, segmentation and thresholding are synonymous.

Thresholding is a method to convert a gray scale image into a binary image so that objects of interest are separated from the background. For thresholding to be effective in object-background separation, it is necessary that the objects and background have sufficient contrast and that we know the intensity levels of either the objects or the background. In a fixed thresholding scheme, these intensity characteristics determined the value of the threshold. In this research, a laser line is an object to be separated from the background. Since a laser line is lighter than the background, an original image $F(u_1,u_2)$ for u_1=1,…,320 and u_2=1,…,240 can be partitioned into the laser line and the background using a thresholding operation as follows:

$$F_T(u_1,u_2) = \begin{cases} 1 & \text{if } F(u_1,u_2) \geq T \\ 0 & \text{otherwise} \end{cases} \tag{2}$$

where $F_T(u_1,u_2)$ is the resulting binary image and T is a threshold. By (2), $F_T(u_1,u_2)$ has 1 for the laser line and 0 for the background. The results of producing an image using different thresholds are shown in Fig. 5. Fig. 5 (b) shows the resulting image with T=150. The left and right sides of the projected laser line is not separated from the background since the intensity values of both sides of the line are outside the interval. For detecting both sides of the line, an image is obtained using T=120 as shown in Fig. 5 (c). As compared with T=150, more parts of the line are detected. Finally, the binary image with T=100 is shown in Fig. 5 (d). Although the resulting image includes more parts of the line as compared with T=150 and T=120, some parts of the background pixels are wrong detected as the line since the intensity of some background pixels are in the interval. As shown in these examples, the threshold of the fixed threshold method should be appropriately determined according to the application domain. In other words, we have to change the threshold whenever the domain is changed. Also, the threshold needs to be changed for an illumination change.

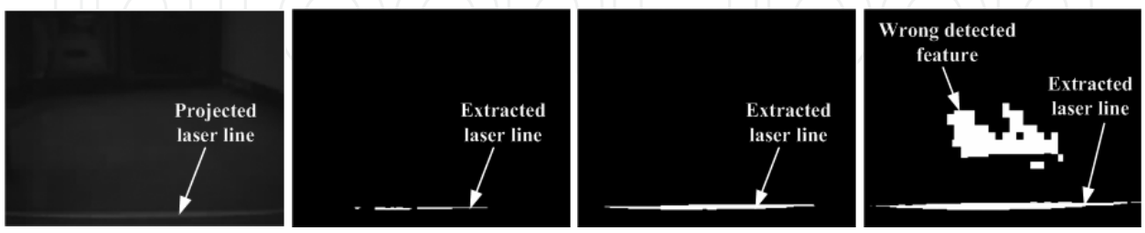

(a) (b) (c) (d)

Fig. 5. Laser-line detection using a fixed threshold scheme: (a) original image, and binary images thresholded with (b) T=150, (c) T=120 and (d) T=100.

In this research, we propose an adaptive vertical threshold scheme in order to separate the laser line from the background regardless of an illumination change. The concept of the proposed

threshold scheme is shown in Fig. 6. Although the intensity of both sides of the line is weaker than the intensity of the center of the line, the artificial laser light is lighter than other pixels on its vertical line. Using this fact, we define a threshold for the uth vertical line as follows:

$$T_V(u) = \max_{u_2} F(u,u_2) \tag{3}$$

where u=1,…,320. As shown in (3), the vertical threshold $T_v(u)$ is adaptively determined as the maximum intensity of the pixels on the uth vertical line even though the intensity of illumination is changed. Using $T_v(u)$, each vertical line is thresholded as follows:

$$F_{VT}(u,u_2) = \begin{cases} 1 & if \quad F(u,u_2) \geq T_V(u) \\ 0 & otherwise \end{cases} \tag{4}$$

Finally, the resulting binary image is obtained by the union of $F_{VT}(u,u_2)$ for u as follows:

$$F_{VT}(u_1,u_2) = \bigcup_{u=1}^{320} F_{VT}(u,u_2) \tag{5}$$

That is, the detected laser line is the region for $F_{VT}(u_1,u_2)$=1. The results of producing an image using the adaptive vertical threshold scheme are shown in Fig. 7. For the low intensity of illumination, the projected laser line is shown in Fig. 7 (a). In this case, the entire laser line is obtained as shown in Fig. 7 (b). For the high intensity of illumination, it is hard to distinguish the laser line from the background as shown in Fig. 7 (c). However, the entire line is also obtained by the proposed vertical threshold scheme as shown in Fig. 7 (d). That is, the adaptive vertical threshold scheme is not sensitive to an illumination change. Thus, the vertical threshold scheme can be directly applied to various application domains.

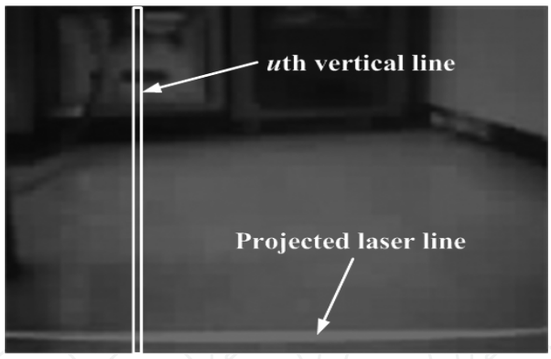

Fig. 6. Concept of an adaptive vertical threshold scheme.

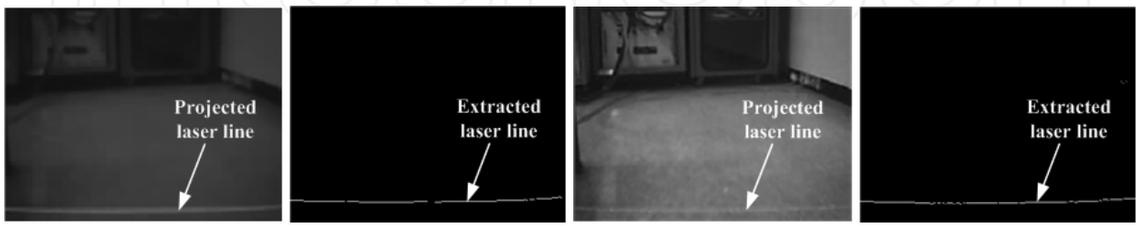

(a) (b) (c) (d)

Fig. 7. Laser-line detection using an adaptive vertical threshold scheme: (a) original image and (b) its vertical thresholded image for low intensity of illumination; (c) original image and (d) its vertical thresholded image for high intensity of illumination.

3.3 Acquisition of 3D Information

In this section, we obtain 3D information from the detected laser line on the 2D camera image using the geometry of the terrain-prediction sensor module. The mobile base frame {*B*} of the agent and the camera frame {*C*} of the terrain prediction sensor with respect to the universal frame {*U*} are depicted in Fig. 8, where the Y_c-axis is set parallel with the Y_b-axis. The X_b-axis of {*B*} is parallel with the heading direction of the agent and the Z_b-axis is normal to the surface of the ground. The Y_b-axis is defined perpendicular to the X_b-Z_b plane and its direction is determined by the right-hand-rule (RHR). The origin of {*B*} is the agent center position (ACP), which is the projected point of the CG on the X_b-Y_b plane. In this research, all other coordinate systems are also defined in accordance with the RHR. According to the relation between {*B*} and {*C*}, point $P_c(x_c,y_c,z_c)\in\boldsymbol{R}^3$ relative to {*C*} can be transformed into point $P_b(x_b,y_b,z_b)\in\boldsymbol{R}^3$ relative to {*B*} as follows:

$$\begin{bmatrix} x_b \\ y_b \\ z_b \\ 1 \end{bmatrix} = \begin{bmatrix} \cos\theta_{bc} & 0 & \sin\theta_{bc} & l_{bc} \\ 0 & 1 & 0 & 0 \\ -\sin\theta_{bc} & 0 & \cos\theta_{bc} & h_{bc} \\ 0 & 0 & 0 & 1 \end{bmatrix} \begin{bmatrix} x_c \\ y_c \\ z_c \\ 1 \end{bmatrix} \tag{6}$$

where l_{bc} and h_{bc} are the translational distances between origins of {*B*} and {*C*} about the X_b-axis and the Z_b-axis, respectively, and θ_{bc} is the angle between {*B*} and {*C*} about the Y_b-axis.

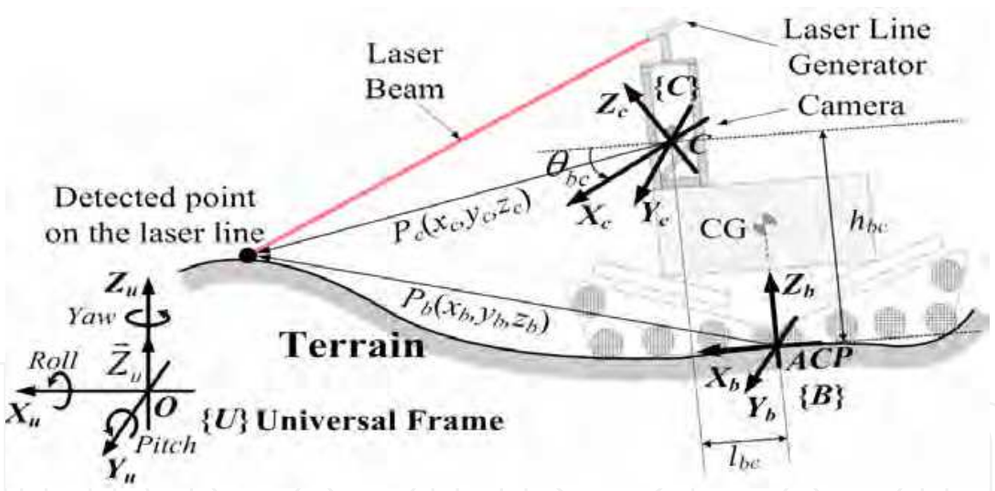

Fig. 8. Transformation of point $P_c(x_c,y_c,z_c)\in\boldsymbol{R}^3$ relative to {C} into point $P_b(x_b,y_b,z_b)\in\boldsymbol{R}^3$ relative to {*B*}.

In Fig. 9, point $P_c(x_c,y_c,z_c)\in\boldsymbol{R}^3$ on the laser line with respect to {*C*} is obtained from point $P_{img}(u_1,u_2)\in\boldsymbol{R}^2$ on the image plane by comparing the similar triangles ΔP_cMC and $\Delta P_{img}M'C$ as follows:

$$\begin{bmatrix} x_c & y_c & z_c \end{bmatrix} = \frac{b'}{f\cot\theta_{lp} + u_2} \begin{bmatrix} f & u_1 & u_2 \end{bmatrix} \tag{7}$$

where f is the focal length of the camera, θ_{lp} is the projection angle of the laser line on the image plane, and b' is the distance between the center of the camera lens C and the

intersection L' of the Z_c-axis and the laser beam. According to the Sine's Law, the distance b' in triangle $\Delta LCL'$ can be obtained as follows:

$$b' = \frac{b \sin(\theta_{lp} - \theta_{bc})}{\sin \theta_{lp}} \tag{8}$$

where b is the baseline distance between the center of the laser line generator L and the camera center C. By (7) and (8), point $P_{img}(u_1,u_2) \in \boldsymbol{R}^2$ on the image plane can be transformed into point $P_b(x_b,y_b,z_b) \in \boldsymbol{R}^3$ relative to $\{B\}$.

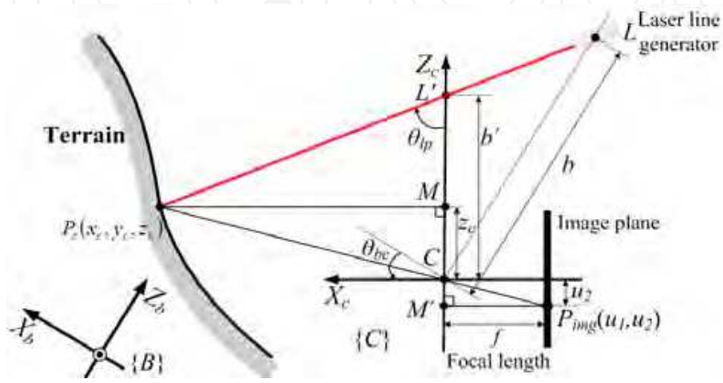

Fig. 9. Geometry between point $P_c(x_c,y_c,z_c) \in \boldsymbol{R}^3$ on the laser line and point $P_{img}(u_1,u_2) \in \boldsymbol{R}^2$ on the image plane relative to $\{C\}$.

3.4 Acquisition of Terrain Parameters

The terrain data at a distance of D_{tr} in front of the agent consist of the roll and pitch angles of the agent set on that terrain. As shown in Fig. 10, the roll angle of the front terrain relative to the current roll angle of the agent is predicted as follows:

$$\Delta\theta_{Roll}(k) = \tan^{-1}\left(\frac{z'_{bL}(k) - z'_{bR}(k)}{D_{track}}\right) \tag{9}$$

where D_{track} is a distance between the right and left tracks of the agent. $P'_{bR}(k)$ and $P'_{bL}(k)$ are the contact points of the right and left tracks with the front terrain at a distance of D_{tr}, where $P'_{bR}(k)$ and $P'_{bL}(k)$ are denoted as $(x'_{bR}(k),y'_{bR}(k),z'_{bR}(k))$ and $(x'_{bL}(k),y'_{bL}(k),z'_{bL}(k))$, respectively. $P'_{bR}(k)$ and $P'_{bL}(k)$ are obtained as following steps:

1. Store the detected points $P_{bR}(k)$ and $P_{bL}(k)$ for the right and left tracks on the laser line and the translational velocity $v(k)$ in the memory at time k.
2. For each time instant, find the minimum times Δk_1 and Δk_2 satisfying the following conditions:

$$x_{bR}(k-\Delta k_1)\cos\left(\theta_{3DM-Pitch}(k-\Delta k_1)\right) - \sum_{n=1}^{\Delta k_1} v(k-n)T_s \cos\left(\theta_{3DM-Pitch}(k-n)\right) < D_{tr} \tag{10}$$

$$x_{bL}(k-\Delta k_2)\cos\left(\theta_{3DM-Pitch}(k-\Delta k_2)\right) - \sum_{n=1}^{\Delta k_2} v(k-n)T_s \cos\left(\theta_{3DM-Pitch}(k-n)\right) < D_{tr} \tag{11}$$

where $\theta_{3DM-Pitch}(k)$ is the pitch angle of the agent obtained by the inclinometer at time k relative to $\{U\}$.

3. Using Δk_1 and Δk_2 satisfying (10) and (11), obtain $P'_{bR}(k)$ and $P'_{bL}(k)$ by the linear interpolation of $P_{bR}(k-\Delta k_1+1)$ and $P_{bR}(k-\Delta k_1)$ and the linear interpolation of $P_{bL}(k-\Delta k_2+1)$ and $P_{bL}(k-\Delta k_2)$, respectively.

Finally, the roll angle relative to $\{U\}$ is obtained from the predicted roll angle $\Delta\theta_{Roll}(k)$ relative to $\{B\}$ as follows:

$$\hat{\theta}_{Roll}(k) = \theta_{3DM-Roll}(k) + \Delta\theta_{Roll}(k) \tag{12}$$

where $\theta_{3DM-Roll}(k)$ is the roll angle of the agent obtained by the inclinometer at time k relative to $\{U\}$.

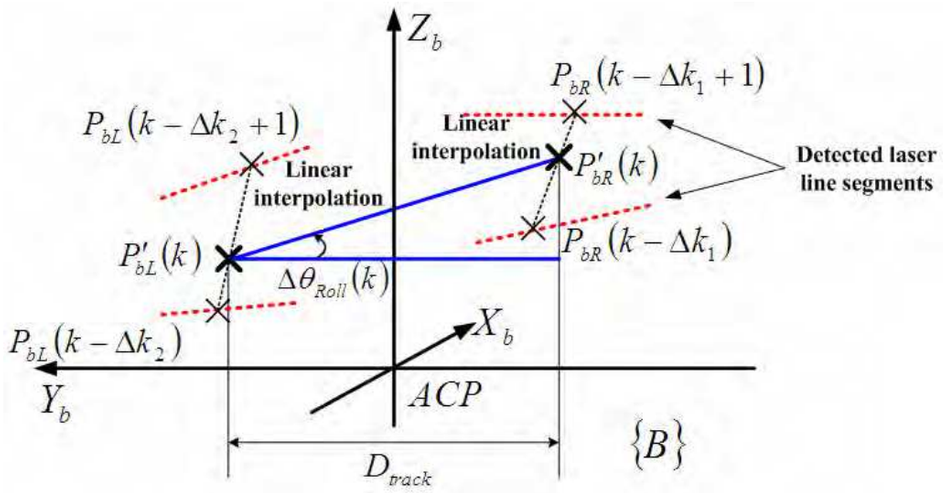

Fig. 10. Predicted roll angle $\Delta\theta_{Roll}(k)$ at a distance of D_{tr} relative to the roll angle at time k by using interpolated points $P'_{bL}(k)$ and $P'_{bR}(k)$ at time k.

As shown in Fig. 11, the pitch angle of the front terrain relative to the current pitch angle of the agent is predicted by the terrain data obtained at times k and $k-\Delta k_3$ as follows:

$$\Delta\theta_{Pitch}(k) = -\tan^{-1}\left(\frac{z'_{bF}(k) - z'_{bF}(k-\Delta k_3)}{x'_{bF}(k) - x'_{bF}(k-\Delta k_3)}\right) \tag{13}$$

where Δk_3 is the minimum time satisfying the condition $L_{fr} \le |P'_{bF}(k)P'_{bF}(k\text{-}\Delta k_3)|$. Here, L_{fr} is the length of the agent tracks, and $|P'_{bF}(k)P'_{bF}(k\text{-}\Delta k_3)|$ is the distance between points $P'_{bF}(k)$ and $P'_{bF}(k\text{-}\Delta k_3)$. Point $P'_{bF}(k)$ is defined by points $P'_{bR}(k)$ and $P'_{bL}(k)$ as follows:

$$\begin{aligned} P'_{bF}(k) &= \left(x'_{bF}(k), y'_{bF}(k), z'_{bF}(k)\right) \\ &= \left(D_{tr}, 0, \frac{z'_{bL}(k) + z'_{bR}(k)}{2}\right) \end{aligned} \tag{14}$$

To obtain the distance $|P'_{bF}(k)P'_{bF}(k\text{-}\Delta k_3)|$, point $P_{bF}(k\text{-}\Delta k_3)$ relative to base frame $\{B(k-\Delta k_3)\}$ defined at time $k-\Delta k_3$ needs to be transformed into point $P'_{bF}(k\text{-}\Delta k_3)$ relative to $\{B(k)\}$ (or $\{B\}$) defined at time k as follows:

$$P'_{bF}(k-\Delta k_3) = P_{bF}(k-\Delta k_3) - \begin{bmatrix} \sum_{n=1}^{\Delta k_3} v(k-n)T_s \cos\left(\theta_{3DM-Pitch}(k-n)\right) \\ 0 \\ -\sum_{n=1}^{\Delta k_3} v(k-n)T_s \sin\left(\theta_{3DM-Pitch}(k-n)\right) \end{bmatrix} \quad (15)$$

The second term on the right-hand side of (15) indicates the displacement vector between $\{B(k-\Delta k_3)\}$ and $\{B(k)\}$. Finally, the pitch angle relative to $\{U\}$ is obtained by the predicted pitch angle $\Delta\theta_{Pitch}(k)$ as follows:

$$\hat{\theta}_{Pitch}(k) = \theta_{3DM-Pitch}(k) + \Delta\theta_{Pitch}(k) \quad (16)$$

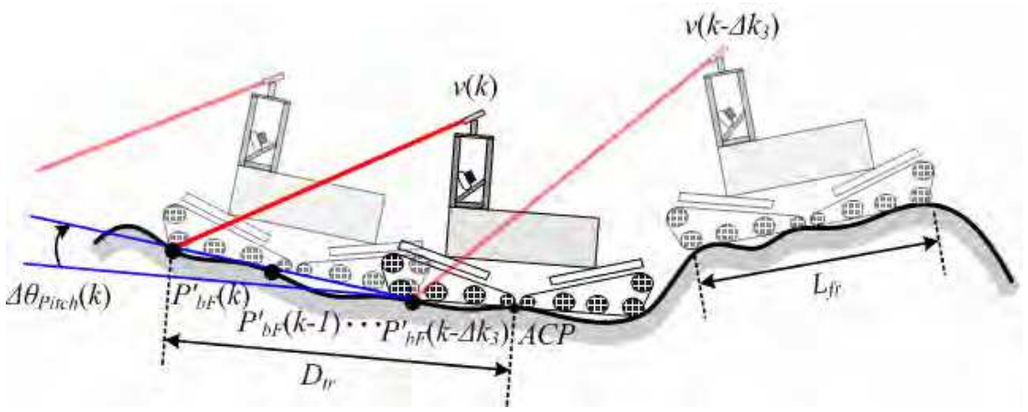

Fig. 11. Predicted pitch angle $\Delta\theta_{Pitch}(k)$ at a distance of D_{tr} relative to the pitch angle at time k by using interpolated points $P'_{bF}(k)$ and $P'_{bF}(k-\Delta k_3)$ at times k and $k-\Delta k_3$, respectively.

4. Turnover Prevention through Prediction

In this section, a turnover prevention algorithm for preventing the agent from pitching over or rolling over is discussed. The pitchover-free range of the translational acceleration and the rollover-free range of the rotational velocity are determined by using the predicted-terrain sensor data. According to both ranges, the translational and rotational velocities of the agent are controlled for pitchover and rollover prevention.

4.1 Dynamics of the Agent

In order to determine turnover constraints for the agent moving through unknown terrain, we adopt the quasi-static rollover analysis of a rigid vehicle (Gillespie, 1992). By assuming the ROBHAZ-DT as a rigid vehicle, the deflections of the suspensions and tracks need not be considered in the analysis. The external forces acting on the agent consist of the friction forces between the vehicle and ground, the normal force, and the gravity force. The total friction force $\boldsymbol{F}$, tangent to the X_b-Y_b plane, can be defined as follows:

$$\boldsymbol{F} = f_{Xb}\boldsymbol{X}_b + f_{Yb}\boldsymbol{Y}_b \quad (17)$$

where f_{Xb} and f_{Yb} are the components tangent and normal to the heading direction of the agent, respectively. By modifying the dynamic-motion equations for the car-like agent

described by Shiller (Shiller, 1991), the motion equation for a differential-drive agent moving through unknown terrain can be described in terms of the translational velocity v and the translational acceleration a as follows:

$$f_{Xb}\mathbf{X}_b+f_{Yb}\mathbf{Y}_b+N\mathbf{Z}_b-mg\mathbf{Z}_u=mv^2/r\mathbf{Y}_b+ma\mathbf{X}_b \tag{18}$$

where N is the magnitude of the normal force in the direction of $\mathbf{Z}_b$, m is the lumped mass of the agent, and r is the turning radius of the agent. Radius r can be represented as v/ω since the agent is a differential-drive vehicle. Parameters f_{Xb} , f_{Yb} and N can be obtained by the dot products of the unit vectors $\mathbf{X}_b$, $\mathbf{Y}_b$ and $\mathbf{Z}_b$ with (18), respectively, as follows:

$$f_{Xb}=mgk_{Xb}+ma \tag{19}$$

$$f_{Yb}=mgk_{Yb}+mv^2/r=mgk_{Yb}+mv\omega \tag{20}$$

$$N=mgk_{Zb} \tag{21}$$

where k_{Xb} , k_{Yb} and k_{Zb} are terrain parameters defined by the projections of unit vector $\mathbf{Z}_u$ on unit vectors $\mathbf{X}_b$, $\mathbf{Y}_b$ and $\mathbf{Z}_b$, respectively. Vector $\mathbf{Z}_u$ is the unit vector $[0\ 0\ 1]^T$ in the opposite direction of the gravity $[0\ 0\ -g]^T$ relative to $\{U\}$. The terrain parameters are represented by the roll and pitch angles of that terrain as follows:

$$k_{Xb}=\mathbf{Z}_u\bullet\mathbf{X}_b=-\sin(\theta_{Pitch}) \tag{22}$$

$$k_{Yb}=\mathbf{Z}_u\bullet\mathbf{Y}_b=\sin(\theta_{Roll})\cos(\theta_{Pitch}) \tag{23}$$

$$k_{Zb}=\mathbf{Z}_u\bullet\mathbf{Z}_b=\cos(\theta_{Roll})\cos(\theta_{Pitch}) \tag{24}$$

where θ_{Roll} and θ_{Pitch} are determined according to the conventional method of the *X-Y-Z fixed angles*.

4.2 Pitchover Prevention Control

The force distribution of the agent is depicted in Figs. 12 (a) and 12 (b) when the agent pitches over CCW and CW about the Y_b-axis, respectively. At the point where the agent is about to pitch over CCW, the total normal force N and the friction force f_{Xb} of the agent are applied on the only front endpoint of the track. Thus the moment on the agent created by those forces should satisfy the condition $f_{Xb}h+NL_{fr}/2\geq 0$ for preventing a pitchover in a CCW direction, where h is the height of the center of gravity (CG) of the agent. In the same way, the moment on the agent should satisfy the condition $f_{Xb}h-NL_{fr}/2\leq 0$ for preventing a pitchover in a CW direction, where forces N and f_{Xb} are applied on the only rear endpoint of the track. The resultant condition for preventing a pitchover can be determined by combining the above conditions as follows:

$$-N\frac{L_{fr}}{2h}\leq f_{X_b}\leq N\frac{L_{fr}}{2h} \tag{25}$$

Substituting (19) and (21) into (25) transforms the resultant condition to an inequality equation in a as follows:

$$-g\left(\frac{L_{fr}}{2h}k_{Z_b}+k_{X_b}\right)\leq a\leq g\left(\frac{L_{fr}}{2h}k_{Z_b}-k_{X_b}\right) \tag{26}$$

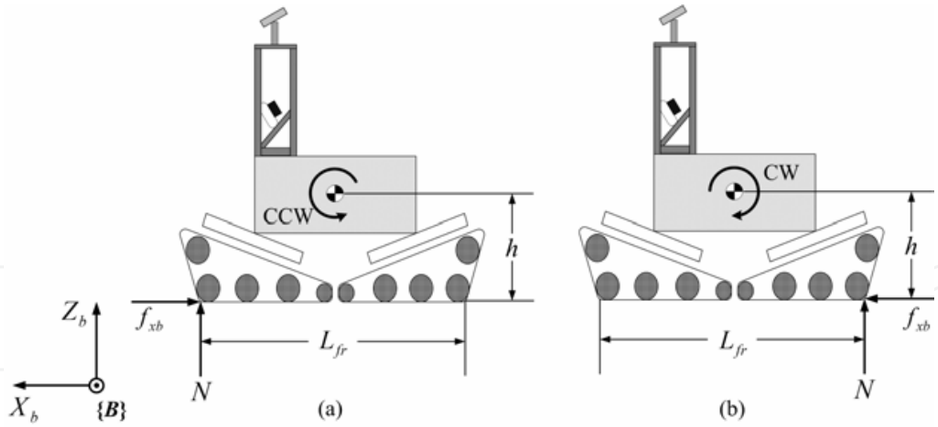

Fig. 12. Force distribution of the agent which is about to pitch over (a) CCW and (b) CW.

Hereafter, the upper and lower bounds of a in (26) are denoted as a_{ub} and a_{lb}, respectively. Bounds a_{ub} and a_{lb} are represented as surfaces in θ_{Roll}-θ_{Pitch}-a space as shown in Fig. 13, where θ_{Roll} and θ_{Pitch} replace k_{Xb} and k_{Zb} in (26). That is, the inner region between the upper and lower surfaces indicates a safe region of the translational acceleration for preventing a pitchover. In this case, the permitted accelerations of the agent for accelerated, uniform and decelerated motions are represented as three planes a=a_c, a=0 and a=−a_c in Fig. 13.

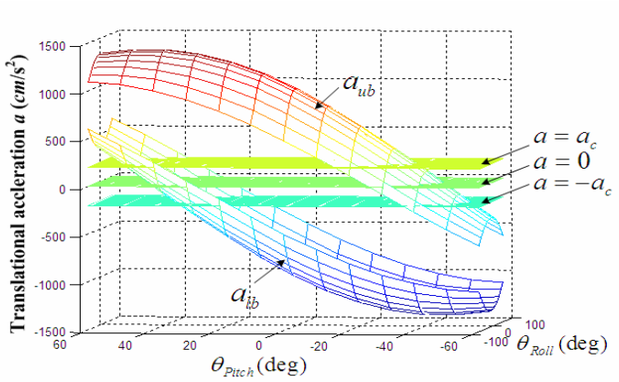

Fig. 13. Graphical analysis of the condition for preventing a pitchover (a_c: normal acceleration of the agent).

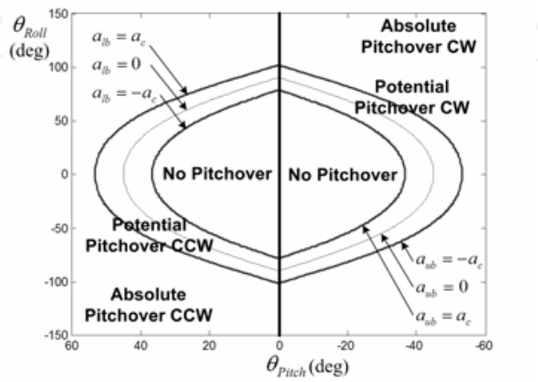

Fig. 14. Five cases for pitchover possibility of the agent according to the roll and pitch angles.

According to the relation of the two surfaces and the three planes, five possible cases of a pitchover are defined as shown in Fig. 14. Each case is determined by the intersection curves of two surfaces with three planes. According to the five cases, the control strategies of the translational velocity for pitchover prevention are described in Table 2. For pitchover prevention control, the pitchover possibility is determined by the front terrain data which are predicted by the terrain-prediction sensor. When the agent detects the terrain for the absolute pitchover CW or CCW case, the agent must decelerate to zero because all permitted accelerations of the agent are beyond the boundary of the safe region of the translational acceleration and thus the agent will unconditionally pitch over at the detected terrain. As a result of deceleration, the agent can stop before arriving at the dangerous terrain. For the potential pitchover CW case, the agent must maintain its velocity or decelerate since it is allowed to only move in uniform and decelerated motions to avoid the CW pitchover. Especially, if the agent detects the terrain where it must decelerate in order to prevent from pitching over CW, it will decelerate and stop before it reaches that terrain. That is, the agent does not enter that pitchover region since it already stops at around the vicinity of the region. On the other hand, in the case of the potential pitchover CCW case, the agent must maintain its velocity or accelerate to avoid the CCW pitchover. In this case, the agent can not accelerate further after its translational velocity reaches the maximum velocity. At this point of view, the agent must decelerate and stop before it arrives at that terrain. The potential pitchover CW case is similar to the potential pitchover CCW case explained before. Finally, in the no pitchover case, the agent is allowed to move in accelerated, uniform and decelerated motions. In other words, the agent need not be controlled for pitchover prevention.

Cases	Permissible acc. ranges	Possible motions		Control strategies
No Pitchover	$-a_c \le a \le a_c$ ($a_{ub} > a_c$ and $a_{lb} < -a_c$)	Accelerated Uniform Decelerated	($a=a_c$) ($a=0$) ($a=-a_c$)	Needless
Potential Pitchover CW	$-a_c \le a \le 0$ ($0 \le a_{ub} < a_c$ and $a_{lb} < -a_c$)	Uniform Decelerated	($a=0$) ($a=-a_c$)	Maintain the translational velocity/ Decelerate to zero
	$-a_c \le a \le -a_c$ ($-a_c \le a_{ub} < 0$ and $a_{lb} < -a_c$)	Decelerated	($a=-a_c$)	
Potential Pitchover CCW	$0 \le a \le a_c$ ($a_{ub} > a_c$ and $-a_c < a_{lb} \le 0$)	Uniform Accelerated	($a=0$) ($a=a_c$)	Decelerate to zero
	$a_c \le a \le a_c$ ($a_{ub} > a_c$ and $0 < a_{lb} \le a_c$)	Accelerated	($a=a_c$)	
Absolute Pitchover (CCW or CW)	None ($a_{ub} < -a_c$ or $a_{lb} > a_c$)	None		Decelerate to zero

Table 2. Control strategies for preventing the pitchover of the agent.

4.3 Rollover Prevention Control

The force distribution of the agent is depicted in Figs. 15 (a) and 15 (b) where the agent rolls over CCW and CW, respectively. In the case where the agent is about to roll over CCW, the total normal force N and the friction force f_{Yb} of the agent are applied on the only left track. Thus, the moment on the agent created by those forces should satisfy the condition $f_{Yb}h+NW_b/2 \ge 0$ for preventing a rollover in a CCW direction. In the same way, the moment on the agent should satisfy the condition $f_{Yb}h-NW_b/2 \le 0$ for preventing a rollover in a CW

direction where the forces N and f_{Yb} are applied on the only right track as shown in Fig. 15 (b). Therefore, the resultant condition to prevent a rollover can be determined by combining the above conditions as follows:

$$-N\frac{W_b/2}{h} \le f_{Y_b} \le N\frac{W_b/2}{h} \tag{27}$$

Substituting (20) and (21) into (27) transforms the resultant condition to an inequality equation in v and ω as follows:

$$-g\left(k_{Y_b}+\frac{W_b/2}{h}k_{Z_b}\right) \le v\omega \le -g\left(k_{Y_b}-\frac{W_b/2}{h}k_{Z_b}\right) \tag{28}$$

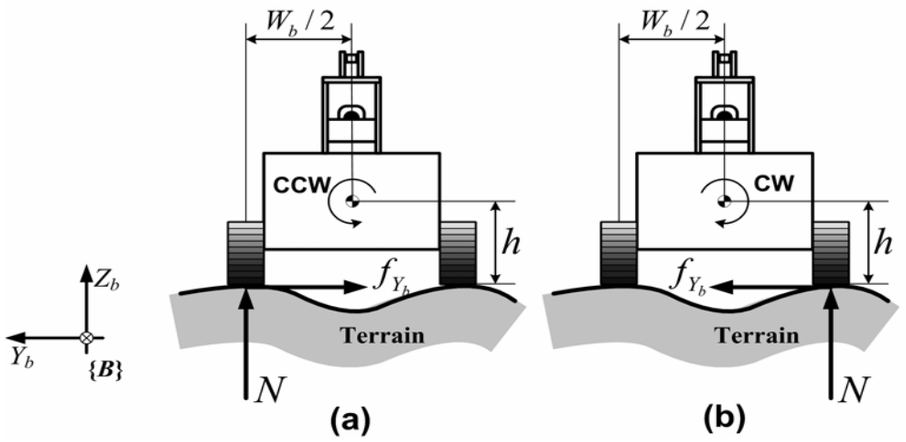

Fig. 15. Force distribution of the agent which is about to roll over (a) CCW and (b) CW.

Hereafter, the upper and lower bounds of $v\omega$ in (28) are denoted as $(v\omega)_{ub}$ and $(v\omega)_{lb}$, respectively. In this case, the translational velocity v is determined by the operator's command and the condition of pitchover prevention. Thus, for the given v, the inequality equation (28) can be represented in terms of ω as follows:

$$\frac{(v\omega)_{lb}}{\min(v+\Delta v, v_{\max})} \le \omega \le \frac{(v\omega)_{ub}}{\min(v+\Delta v, v_{\max})} \tag{29}$$

where Δv is the maximum increase of the translational velocity while the agent is moving the distance of D_{tr}: $\Delta v = -v + (v^2 + 2a_c D_{tr})^{1/2}$. Due to the motor torque constraints, translational velocity $v+\Delta v$ is restricted by $v_{\max}$. Here, the upper and lower bounds in (29) are denoted as ω_{ub} and ω_{lb}, respectively. The rollover-free region of the rotational velocity is defined as the inner region between surfaces ω_{ub} and ω_{lb} in θ_{Roll}-θ_{Pitch}-ω space as shown in Fig. 16. In this figure, three planes $\omega=\omega_{\max}$, $\omega=0$ and $\omega=-\omega_{\max}$ for the rotational velocity are also depicted with the surfaces, where $\omega_{\max}$ is the maximum rotational velocity of the agent. According to the relation of the two surfaces and the three planes, the control regions for rollover prevention are defined as shown in Fig. 17. The boundaries b_{ui} and b_{lj} for i,j=1,2,3 are determined by the intersection curves of surfaces ω_{ub} and ω_{lb} with the three planes, respectively. According to the five control regions, the control strategies of the translational and rotational velocities for rollover prevention are described in Table 3. For the free moving region A, the rotational velocity of the agent can be determined for the

entire permissible range from $-\omega_{max}$ to ω_{max}. That is, the operator can control the agent with no restriction for the rotational velocity. On the contrary, for the restricted regions B1 and B2, the rotational velocity must be restricted for preventing a rollover. If the detected terrain is in B1, the rotational velocity is truncated to range from $-\omega_{max}$ to ω_{ub} since $\omega_{ub}<\omega_{max}$. Especially, for the region between b_{u2} and b_{u3}, the agent is allowed to only turn right since $\omega_{ub}<0$. In other words, the agent cannot turn left and go straight. For the region B2, the rotational velocity is truncated to range from ω_{lb} to ω_{max} since $-\omega_{max}<\omega_{lb}$. Similarly to the case of B1, for the region between b_{l2} and b_{l3}, the agent is allowed to only turn left since $\omega_{ub}<0$. Finally, if the detected terrain is in the uncontrollable regions C1 and C2, the agent must stop before arriving at that terrain because the whole range from $-\omega_{max}$ to ω_{max} is beyond the safe range from ω_{ub} to ω_{lb} and the agent will unconditionally roll over at that terrain.

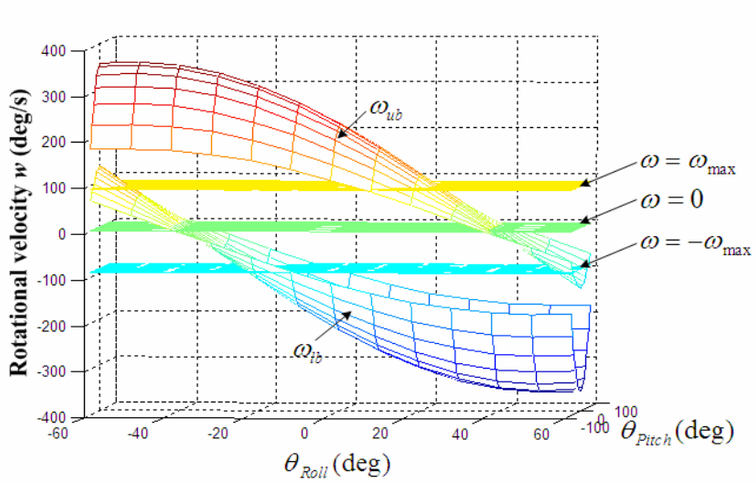

Fig. 16. Graphical analysis of the condition for preventing a rollover (ω_{max}: maximum rotational velocity of the agent).

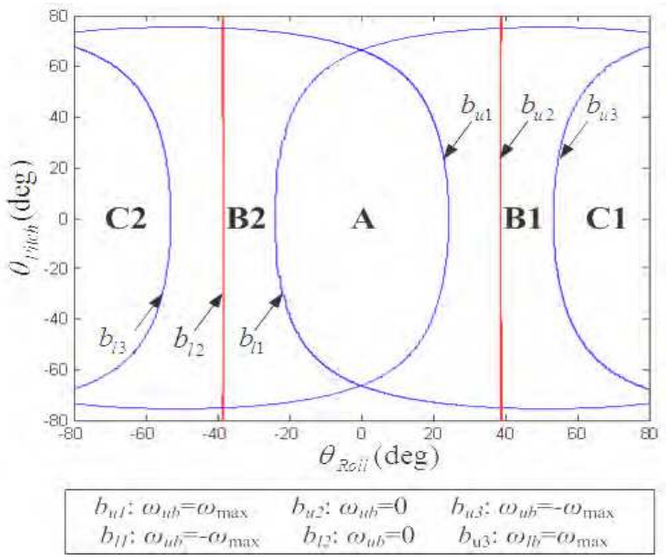

Fig. 17. Control regions for rollover prevention according to roll and pitch angles (A: free moving region; B1, B2: restricted regions; C1, C2: uncontrollable regions).

Control regions	Rollover-free ranges of the rotational vel.	Control strategies
Free moving region A	$-\omega_{max} \le \omega \le \omega_{max}$ ($\omega_{ub} \ge \omega_{max}$ and $\omega_{lb} \le -\omega_{max}$)	Needless
Restricted region B1	$-\omega_{max} \le \omega \le \omega_{ub}$ ($\omega_{ub} < \omega_{max}$ and $\omega_{lb} \le -\omega_{max}$)	Restrict the rotational velocity by ω_{ub}
Restricted region B2	$\omega_{lb} \le \omega \le \omega_{max}$ ($\omega_{ub} \ge \omega_{max}$ and $\omega_{lb} > -\omega_{max}$)	Restrict the rotational velocity by ω_{lb}
Uncontrollable region C1	None ($\omega_{ub} < -\omega_{max}$)	Reduce the translational velocity to zero/Stop
Uncontrollable region C2	None ($\omega_{lb} > \omega_{max}$)	Reduce the translational velocity to zero/Stop

Table 3. Control strategies for preventing the rollover of the agent.

5. Reflective Force Generation

5.1 Force Reflection System

It is possible that turnover prevention control can cause inconsistencies between the driving command of the operator and the reactive motion of the agent. Thus, a reflective force is generated to compensate the inconsistencies. The experimental setup for force reflection is depicted in Fig. 18. The WingMan Force Pro joystick of Logitech is employed as a 2 DOF force feedback joystick which not only receives a command of an operator but also generates a reflective force. The joystick interface is developed by using the Microsoft DirectX 8.0 Software Development Kit (SDK). The positions about the *X*-axis and the *Y*-axis of the joystick coordinates determine the rotational and translational velocities of the agent, respectively.

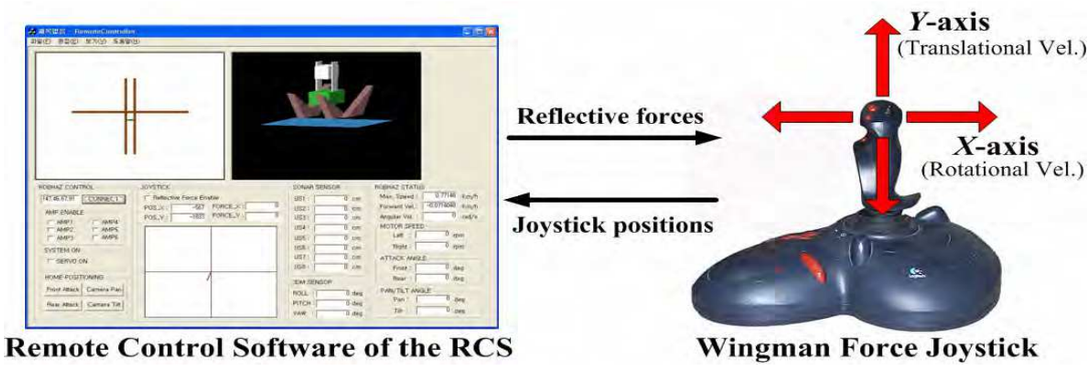

Fig. 18. Experimental setup for force reflection with the Logitech Wingman Force Pro joystick.

5.2 Position-based Reflective Force for Turnover Prevention

The position-based force $\mathbf{F}_R$ is depicted in Fig. 19. The force $\mathbf{F}_R$ is determined by the position $\mathbf{q}$ about the axis of the joystick coordinates as follows:

$$\mathbf{F_R} = \begin{cases} -\mathbf{k}_{NC} \cdot [\mathbf{q} - (\mathbf{q}_{offset} - \mathbf{W}_{DB})], & \mathbf{q} < (\mathbf{q}_{offset} - \mathbf{W}_{DB}) \\ -\mathbf{k}_{PC} \cdot [\mathbf{q} - (\mathbf{q}_{offset} + \mathbf{W}_{DB})], & \mathbf{q} > (\mathbf{q}_{offset} + \mathbf{W}_{DB}) \end{cases} \quad (30)$$

where the parameters of the position-based force are described in Table 4. If $\mathbf{q}$ is apart from $\mathbf{q}_{offset}$, the reflective force is generated for pushing the joystick to $\mathbf{q}_{offset}$. In other words, the position-based force makes it difficult for the operator to push the joystick far from $\mathbf{q}_{offset}$. The force parameters $\mathbf{F}_{PS}$ and $\mathbf{k}_{PC}$ for $\mathbf{q}>\mathbf{q}_{offset}$ and the parameters $\mathbf{F}_{NS}$ and $\mathbf{k}_{NC}$ for $\mathbf{q}<\mathbf{q}_{offset}$ can be determined independently. In addition, as the dead-band for the reflective force can be defined by $\mathbf{W}_{DB}$ around $\mathbf{q}_{offset}$, no reflective force is generated if $\mathbf{q}$ is located between $(\mathbf{q}_{offset}-\mathbf{W}_{DB})$ and $(\mathbf{q}_{offset}+\mathbf{W}_{DB})$. Thus, the sensitivity to a slight displacement of $\mathbf{q}$ around $\mathbf{q}_{offset}$ can be reduced.

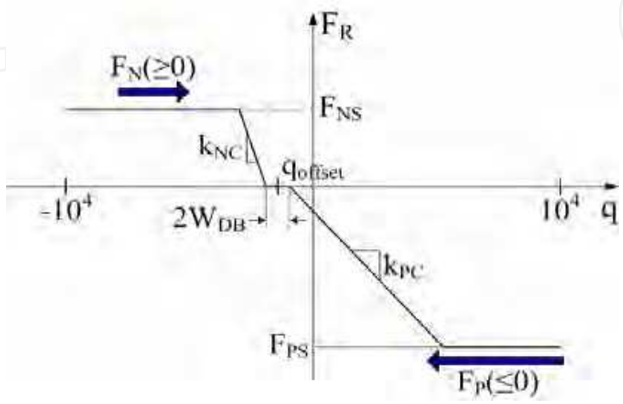

Fig. 19. Parameters of the position-based force $\mathbf{F}_R$ for the joystick position $\mathbf{q}$.

Parameters	Descriptions	Ranges	
		(from)	(to)
$\mathbf{q}_{offset}$	Reference position of the position-based force	-10^4	10^4
$\mathbf{W}_{DB}$	Dead-band defined relative to $\mathbf{q}_{offset}$, where no force is generated	0	10^4
$\mathbf{k}_{NC}$	Proportional factor of the force on the negative side of $\mathbf{q}_{offset}$ when $\mathbf{q}<(\mathbf{q}_{offset}-\mathbf{W}_{DB})$	-10^4	10^4
$\mathbf{k}_{PC}$	Proportional factor of the force on the positive side of $\mathbf{q}_{offset}$ when $\mathbf{q}>(\mathbf{q}_{offset}-\mathbf{W}_{DB})$	-10^4	10^4
$\mathbf{F}_{NS}$	The maximum force on the negative side of $\mathbf{q}_{offset}$	-10^4	10^4
$\mathbf{F}_{PS}$	The maximum force on the positive side of $\mathbf{q}_{offset}$	-10^4	10^4

Table 4. Parameters of the position-based reflective force.

For pitchover prevention, the reflective force about the *Y*-axis of the joystick coordinates is generated as shown in Fig. 20 (a). As described in Section 4.2, if the agent detects pitchovers at front terrain, it must keep its translational velocity or decelerate to zero to avoid a pitchover. That is, the desired translational velocity v_d for pitchover prevention is set as the current translational velocity of the agent or decreased continuously. Through the reflective force, the operator recognizes that the translational velocity is restricted by v_d. If the operator pushes the joystick in the positive direction above the joystick position for v_d, he/she will feel a repulsive force in the negative direction. On the other hand, if the operator pulls the joystick in the negative direction below the joystick position for v_d, he/she will feel no reflective force. Therefore, the operator can recognize the upper limit v_d for pitchover prevention by the repulsive force. The parameters of the reflective force are determined as $\mathbf{q}_{offset}=f_1(v_d)$, $\mathbf{W}_{DB}=10^2$, $\mathbf{F}_{NS}=0$, $\mathbf{F}_{PS}=10^4$, $\mathbf{k}_{NS}=0$ and $\mathbf{k}_{PS}=10^4$, where $f_1(\cdot)$ is a mapping function

of the desired translational velocity onto the joystick position. In this case, the only $\mathbf{q}_{\text{offset}}$ is changed according to the desired translational velocity v_d for pitchover prevention.
For rollover prevention, a reflective force about the *X*-axis is generated as shown in Fig. 20 (b). If the agent detects a possible rollover at the front terrain, the safety range of its rotational velocity is determined to avoid rollovers as discussed in Section 4.3. The operator can detect the safety range through the reflective force while driving the agent. If the operator maneuvers the agent within this safety range of the rotational velocity, no reflective force is generated. Thus, the operator can drive the agent without any restriction. However, if the operator pushes the joystick beyond the safety region, he will feel a reflective force which pushes the joystick in the direction of the safety region. That is, if the operator pushes the joystick above the joystick position for the upper bound of the safety region, the reflective force in the negative direction is generated to prevent from being pushed in the positive direction. Also, in the case where the operator pushes the joystick below the joystick position for the lower bound of the safety region, the reflective force in the positive direction is generated to prevent from being pushed in the negative direction. The parameters $\mathbf{q}_{\text{offset}}$ and $\mathbf{W}_{\text{DB}}$ of the reflective force about the *X*-axis are determined according to the safety region of the rotational velocity as follows:

$$\begin{aligned}\mathbf{q}_{\text{offset}} &= f_2(\omega_{lb}, \omega_{ub}) \\ &= 10^4 \cdot \frac{1}{2} \cdot \frac{\left[\max(\omega_{lb}, -\omega_{\max}) + \min(\omega_{ub}, \omega_{\max})\right]}{\omega_{\max}}\end{aligned} \tag{31}$$

$$\begin{aligned}\mathbf{W}_{\text{DB}} &= f_3(\omega_{lb}, \omega_{ub}) \\ &= 10^4 \cdot \frac{1}{2} \cdot \frac{\left[\min(\omega_{ub}, \omega_{\max}) - \max(\omega_{lb}, -\omega_{\max})\right]}{\omega_{\max}}\end{aligned} \tag{32}$$

where $f_2(\cdot)$ is a mapping function of the center of the safety region onto the joystick position and $f_3(\cdot)$ is a mapping function of the width of the safety region onto the dead-band of the reflective force. The other parameters are determined as $\mathbf{F}_{\text{NS}}=10^4$, $\mathbf{F}_{\text{PS}}=10^4$, $\mathbf{k}_{\text{NS}}=10^4$ and $\mathbf{k}_{\text{PS}}=10^4$. In this case, the parameters $\mathbf{q}_{\text{offset}}$ and $\mathbf{W}_{\text{DB}}$ are changed according to the safety region for rollover prevention. As a result of reflective force generation, the operator can intuitively determine how to drive the agent for turnover prevention.

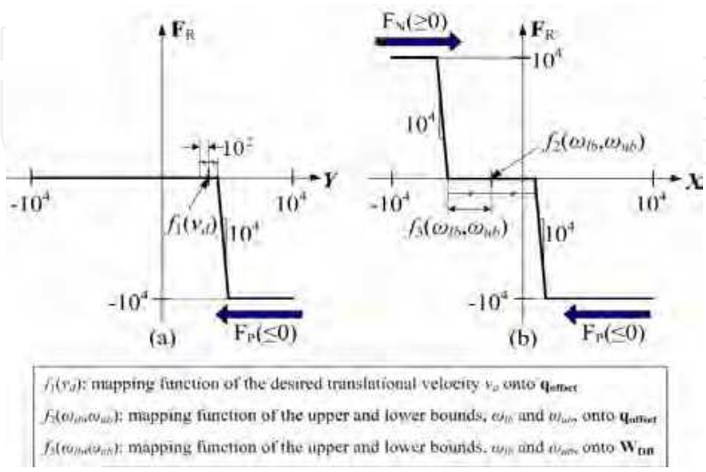

Fig. 20. Reflective forces for recognizing (a) the desired translational velocity for pitchover prevention and (b) the safe region of the rotational velocity for rollover prevention.

6. Experimental Results

Two experiments were carried out with the ROBHAZ-DT in order to verify the feasibility of the proposed turnover prevention algorithm. The sampling time T_s was set as 100 ms. Two resultant paths of the agent moving on the sloped terrain are depicted in Fig. 21. The system parameters for the experiments are described in Table 5.

Parameters	Descriptions
v_{max}=860	The maximum translational velocity [mm/s]
ω_{max}=90	The maximum rotational velocity [°/s]
a_c=1500	The normal acceleration [mm/s^2]
W_b=48	The width between two tracks of the agent [cm]
h_1=25, h_2=70	The height of the center of gravity of the agent [cm]
D_{tr}=68	The reference distance for the turnover prevention [cm]

Table 5. System parameters for the experiments about turnover prevention.

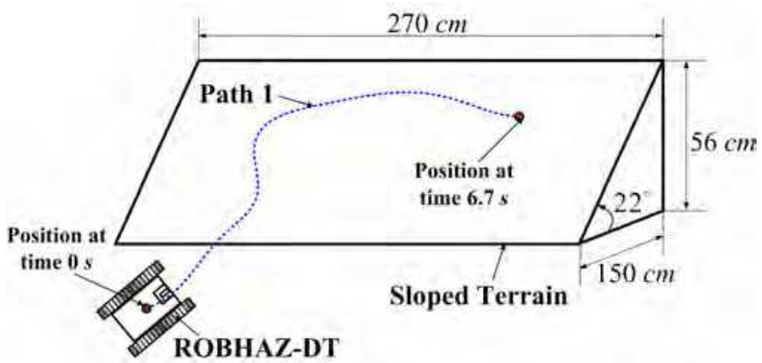

(a)

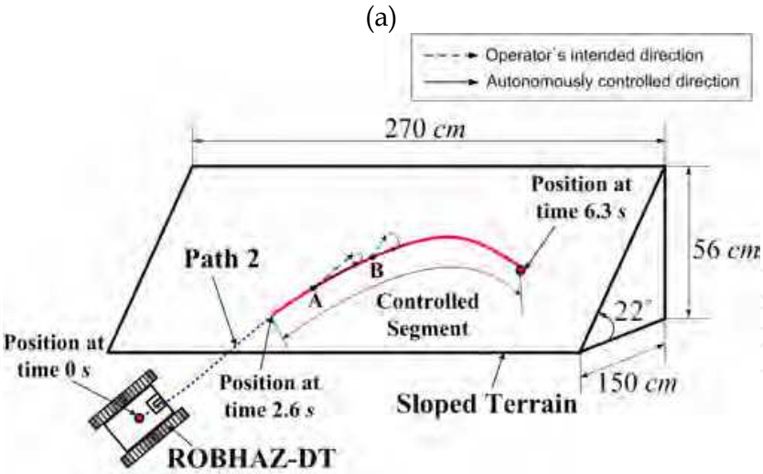

(b)

Fig. 21. Resultant paths of the ROBHAZ-DT moving on the sloped terrain: (a) Path1 for h_1=25 cm, and (b) Path2 for h_2=70 cm where the solid line segment indicates the controlled path for turnover prevention.

The first experiment was carried out with an only mobile base of the ROBHAZ-DT, where h_1=25 cm. The agent moved for 6.7 s as shown in Path1 of Fig. 21 (a). The terrain data at a distance of D_{tr} in front of the agent are depicted in Fig. 22 (a). These terrain data were

predicted by the terrain-prediction sensor and used for turnover prevention. In this experiment, no turnover was detected in the front terrain and thus the translational and rotational velocities of the agent need not be controlled for turnover prevention. That is, the desired translational velocity v_d for pitchover prevention was set as the maximum translational velocity $v_{\max}$ and the safety region of the rotational velocity covered the whole range of the rotational velocity of the agent as shown in Fig. 22 (b). Also, reflective force for turnover prevention was not generated and thus the operator could freely control the agent as shown in Figs.22 (c) and 22 (d).

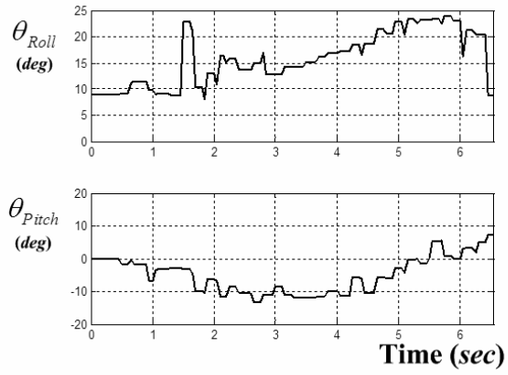

(a)

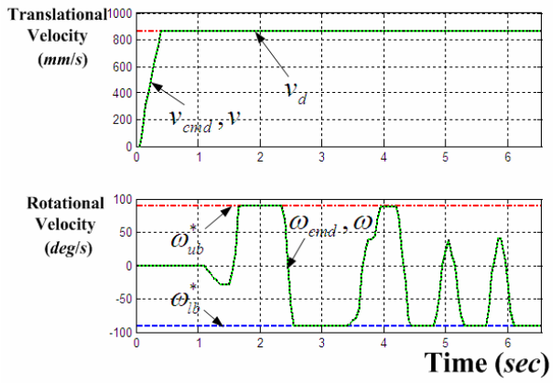

(b)

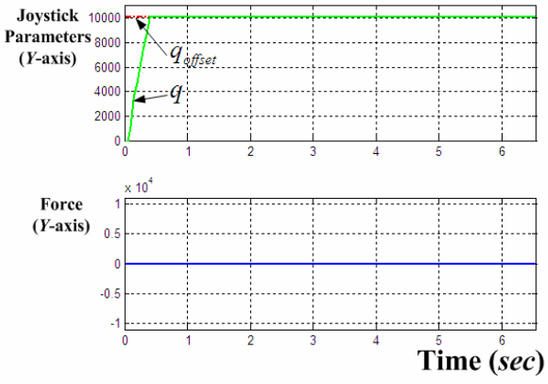

(c)

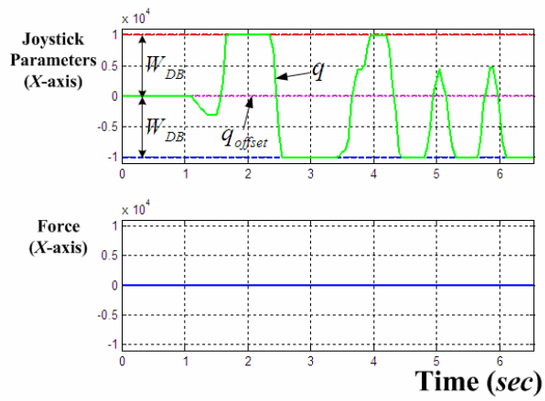

(d)

Fig. 22. Experimental results about turnover prevention (W_b=48 cm and h_1=25 cm): (a) Terrain parameters at a distance of D_{tr} in front of the agent, (b) rotational and translational velocities, (c) joystick parameters about the *Y*-axis, and (d) joystick parameters about the *X*-axis.

The second experiment was carried out using the mobile base with a manipulator. In this experiment, we assumed that the configuration of the manipulator was fixed while the agent was in motion since the action of the manipulator might bring about a change of the center of gravity (CG) of the agent. In this case, although the CG of the agent was not changed, the height of the CG rose up to h_2=70 cm due to the mass of the manipulator attached to the mobile base. In the second experiment, the agent moved for 6.3 s as shown in Path2 of Fig. 21 (b). The solid line segment of Path2 indicates that the agent was autonomously controlled for turnover prevention. Especially, at A and B of Path2, the intended direction of the operator is modified for turnover prevention. If the agent is still controlled by the operator at A and B, it will overturn soon.

The terrain data at a distance of D_{tr} in front of the agent are depicted in Fig. 23 (a). In this case, the agent detected turnovers in the front terrain and thus the translational and rotational velocities of the agent were controlled as shown in Fig. 23 (b). For the given terrain data at each time instant, the desired translational velocity v_d was autonomously controlled for pitchover prevention and the translational velocity v_{cmd} of the operator's command was restricted by v_d. As shown in Fig. 23 (b), the resultant translational velocity v was decelerated by $-a_c$ and accelerated by a_c to follow the desired velocity v_d. Also, the upper bound ω_{ub} of the safety region of the rotational velocity was determined for rollover prevention and the rotational velocity ω_{cmd} of the operator's command was restricted by ω_{ub}. At A and B of Fig. 23 (b), the resultant rotational velocity ω was restricted by ω_{ub}, since ω_{cmd} exceeded ω_{ub}. Here, A and B of Fig. 23 (b) correspond to A and B of Fig. 21 (b), respectively. As shown in Fig. 23 (c), when the joystick position for v_{cmd} exceeded v_d, the reflective force about the *Y*-axis was generated in the negative direction. As a result, the operator felt a repulsive force preventing him/her from pushing above the position for v_d, and hence recognized that the translational velocity of the agent was restricted by v_d for pitchover prevention. Also, when the joystick position for ω_{cmd} exceeded the upper bound of the safety region, the reflective force about the *X*-axis was generated in the negative direction and vice versa. Thus, through the reflective force, the operator could intuitively recognize the safety region of the rotational velocity for rollover prevention and thus be guided to control the rotational velocity within the safety range.

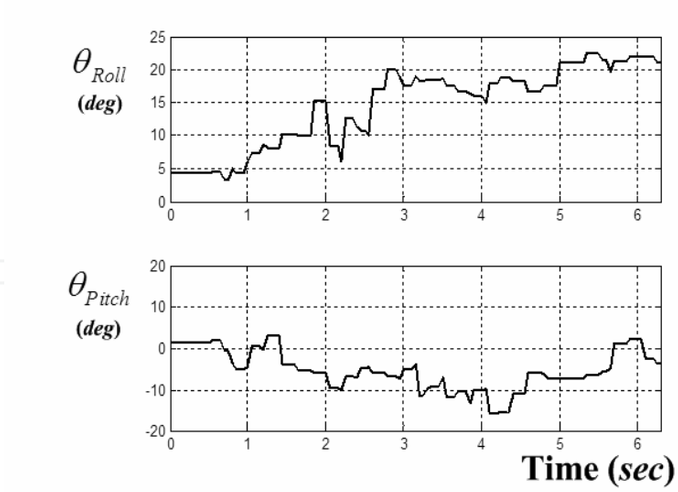
θ_{Roll} (deg)
θ_{Pitch} (deg)
Time (sec)

(a)

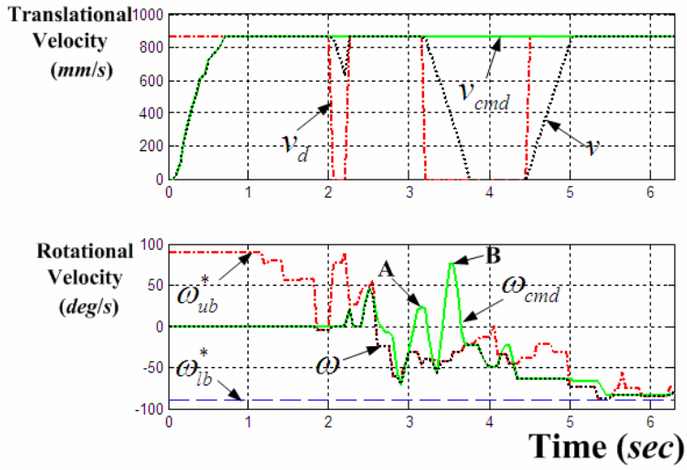
Translational Velocity (mm/s)
v_d
v_{cmd}
v
Rotational Velocity (deg/s)
ω^*_{ub}
ω^*_{lb}
ω
ω_{cmd}
A
B
Time (sec)

(b)

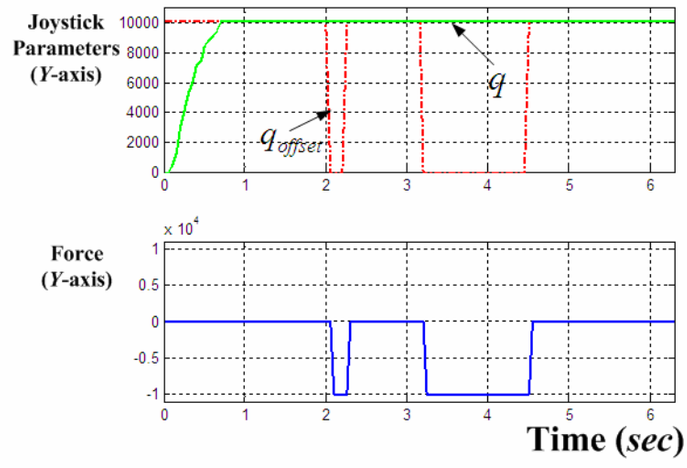
Joystick Parameters (Y-axis)
q_{offset}
q
Force (Y-axis)
x 10^4
Time (sec)

(c)

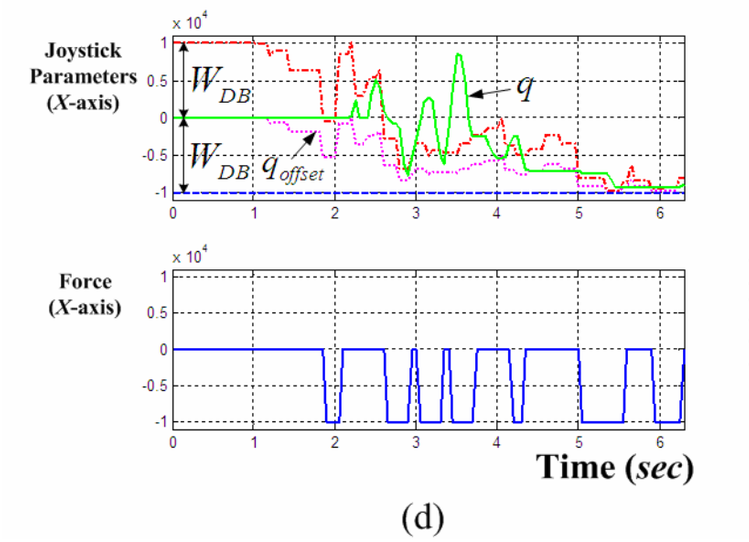

Fig. 23. Experimental results about turnover prevention (W_b=48 cm and h_2=70 cm): (a) Terrain parameters at a distance of D_{tr} in front of the agent, (b) rotational and translational velocities, (c) joystick parameters about the *Y*-axis, and (d) joystick parameters about the *X*-axis.

7. Conclusions

The turnover prevention control algorithm of a teleoperated mobile agent was presented. For online prediction of front terrain, a low-cost terrain prediction sensor composed of a camera vision, a laser line generator, and an inclinometer was developed. The terrain parameters were obtained by finding structured laser line projected onto the front terrain and used for turnover prevention control through the quasi-static rollover analysis. As a result of turnover prevention control, the translational and rotational velocities of the agent were restricted. However, the velocity restriction for turnover prevention may bring about the inconsistencies between the intended motion and the reactive motion of the agent. Thus, the force reflection technique was proposed in order to compensate the inconsistencies. Through the position-based reflective force, the operator could intuitively recognize how the agent should be controlled to avoid turnovers. Finally, based on the experimental results, we found that the agent can even avoid turnovers in unknown sloped terrain.

8. Future Works

In future works, the proposed algorithm for a mobile manipulator with a moving manipulator will be studied. As the manipulator motion brings about a change of center of gravity, a change of the center of gravity of the agent needs to be considered simultaneously.

9. Acknowledgement

This works was supported in part by the Korea Institute of Science and Technology, in part by the Science Research Center/Engineering Research Center program of Ministry of Science and Technology/Korea Science and Engineering Foundation under Grant R11-1999-008, and in part by the Automation and Systems Research Institute.

10. References

Acarman, T. & Özgüner, Ü. (2003). Rollover prevention for heavy trucks using frequency shaped sliding mode control. *IEEE International Conference on Control Application*, pp.7-12, Istanbul, Turkey, June, 2003

Ando, N.; Korondi, P. & Hashimoto, H. (2001). Development of micromanipulator and haptic interface for networked micromanipulation. *IEEE Transactions on Mechatronics*, Vol.6, No.4, 2001, pp.417-427

Basdogan, C.; De, S. & Kim, J. (2004). Haptics in minimally invasive surgical simulation and training. *IEEE Computer Graphics and Applications*, Vol.24, No.2, 2004, pp.56-64

Borenstein, J. & Koren, Y. (1989). Real-time obstacle avoidance for fast mobile robots. *IEEE Transactions on Systems, Man, and Cybernetics*, Vol.19, No. 15, September/October, 1989, pp. 1179-1187

Borenstein, J. & Koren, Y. (1991a). The vector field histogram-Fast obstacle avoidance for mobile robots. *IEEE Transactions on Robotics and Automation*, Vol.7, No.3, June, 1991, pp.278-288

Borenstein, J. & Koren, Y. (1991b). Histogramic in-motion mapping for mobile robot obstacle avoidance. *IEEE Transactions on Robotics and Automation*, Vol.7, No.4, August, 1991, pp.535-539

Boukhnifer, M.; Ferreira, A. & Fontaine, J. (2004). Scaled teleoperation controller design for micromanipulation over internet. *IEEE International Conference on Robotics and Automation*, pp.4577-4583, New Orleans, LA, USA, April, 2004

Chen, B. & Peng, H. (1999). A real-time rollover threat index for sports utility vehicles. *American Control Conference*, pp.1233-1237, San Diego, CA, June, 1999

Chen, E. & Marcus, B. (1998). Force feedback for surgical simulation. *Invited paper, Proceedings of IEEE*, Vol.86, No.3, pp.524-530, March, 1998

Gillespie, T. (1992). *Fundamentals of Vehicle Dynamics*. Warrendale, PA: Society of Automotive Engineers, Inc., 1992

Howard, A. & Seraji, H. (2001). An intelligent terrain-based navigation system for planetary rovers. *IEEE Robotics and Automation Magazine*, Vol.8, No.4, 2001, pp.9-17

Huang, Q.; Sugano, S. & Tanie, K. (1994). Stability control for a mobile manipulator using a potential method. *IEEE International Conference on Intelligent Robots and Systems*, pp.839-846, Munich, Germany, September, 1994

Huang, Q.; Sugano, S. & Kato, I. (1994). Stability compensation of a mobile manipulator by manipulator motion: Feasibility and planning. *IEEE International Conference on Intelligent Robots and Systems*, pp.1285-1292, Grenoble, France, September, 1997

Jain, B.; Kasturi, R. & Schunck, B. (1995). *Machine Vision*, New York: McGraw-Hill

Kim, J.; Lee, H. & Yang, M. (2002). Robotic contamination cleaning system. *IEEE International Conference on Intelligent Robots and Systems*, pp.1874-1879, Lausanne, Switzerland, October, 2002

Lin, Q. & Kuo, C. (1997). Virtual tele-operation of underwater robots, *IEEE International Conference on Robotics and Automation*, pp.1022-1027, Albuquerque, NM, USA, 1997

Nalecz, A. & Bindenmann, A. (1987). Sensitivity analysis of vehicle design attributes that affect vehicle response in critical accident situations-Part I: User's manual. *DOT-HS-807-229*, Washington, D.C.: Department of Transportation, 1987

Nalecz, A. (1991). Intermediate maneuver induced rollover simulation (IMIRS)-A sensitivity analysis. *DOT-HS-807-672*, Washington, D.C.: Department of Transportation, February, 1991

Nalecz, A.; Lu, A. & d'Entremont, K. (1993). An investigation into dynamic measures of vehicle rollover propensity. *SAE Technical Paper 930831*, Detroit, MI: Society of Automotive Engineers, 1993

Niwa, Y.; Yukita, S. & Hanaizumi, H. (2004). Depthmap-based obstacle avoidance on rough terrain. *IEEE International Conference on Intelligent Robotics and Systems*, pp.1612-1617, Sendai, Japan, September, 2004

Nudehi, S.; Mukherjee, R. & Ghodoussi, M. (2005). A shared-control approach to haptic interface design for minimally invasive telesurgical training. *IEEE Transactions on Control Systems Technology*, Vol.13, No.4, 2005, pp.588-592

Papadopoulos, G. & Rey, D. (1996). A new measure of tipover stability margin for mobile manipulators. *IEEE International Conference on Robotics and Automation*, pp.3111-3116, Minneapolis, MN, April, 1996

Park, J.; Lee, B. & Chung, W. (2003a). Reflective force navigation control for a mobile robot using a state transition diagram. *IEEE International Conference on Advanced Intelligent Mechatronics*, pp.52-57, Kobe, Japan, July, 2003

Park, J.; Lee, B. & Kim, M. (2003b). Remote control of a mobile robot using distance-based reflective force. *IEEE International Conference on Robotics and Automation*, pp.600-605, Taipei, Taiwan, R.O.C., September, 2003

Park, J. & Lee, B. (2004). Reflective force integration method for nonautonomous mobile robot control. *IEEE International Conference on Robotics and Automation*, pp.3950-3955, New Orleans, LA, USA, April, 2004

Park, J.; Lee, J. & Lee, B. (2006a). Online turnover-free control for a mobile agent with a terrain prediction sensor. *Journal of Field Robotics*, Vol.23, Issue 1, January, 2006, pp.59-77

Park, J.; Lee, J. & Lee, B. (2006b). Rollover-free navigation for a mobile agent in an unstructured environment. *IEEE Transactions on Systems, Man, and Cybernetics-Part B*, Vol.36, No.4, August, 2006, pp.835-848

Rey, A. & Papadopoulos, E. (1997). Online automatic tipover prevention for mobile manipulators. *IEEE International Conference on Intelligent Robots and Systems*, pp.1273-1278, Grenoble, France, September, 1997

Shiller, Z. & Gwo, Y. (1991). Dynamic motion planning of autonomous vehicles. *IEEE Transctions on Robotics and Automation*, Vol.7, No.2, April, 1991, pp.241-249

Singh, S.; Simmons, R.; Smith, T.; Stentz, A.; Verma, V.; Yahja, A. & Schwehr, K. (2000). Recent progress in local and global traversability for planetary rovers. IEEE International Conference on Robotics and Automation, pp.1194-1200, San Francisco, CA, April, 2000

Smith, F.; Backman, D. & Jacbsen, S. (1992). Telerobotic manipulator for hazardous environments. *Journal of Robotic Systems*, Vol.9, No.2, 1992, pp.251-260

Sugano, S.; Huang, Q. & Kato, I. (1993). Stability criteria in controlling mobile robotic systems. *IEEE International Conference on Intelligent Robots and Systems*, pp.832-838, Yokohama, Japan, July 1993

Takano, S. & Nagai, M. (2001). Dynamics control of large vehicles for rollover prevention. *IEEE International Conference on Vehicle Electronics*, pp.85-89, Tottori, Japan, September, 2001

Mobile Robotics, Moving Intelligence

Edited by Jonas Buchli

ISBN 3-86611-284-X

Hard cover, 586 pages

Publisher Pro Literatur Verlag, Germany / ARS, Austria

Published online 01, December, 2006

Published in print edition December, 2006

This book covers many aspects of the exciting research in mobile robotics. It deals with different aspects of the control problem, especially also under uncertainty and faults. Mechanical design issues are discussed along with new sensor and actuator concepts. Games like soccer are a good example which comprise many of the aforementioned challenges in a single comprehensive and in the same time entertaining framework. Thus, the book comprises contributions dealing with aspects of the Robotcup competition. The reader will get a feel how the problems cover virtually all engineering disciplines ranging from theoretical research to very application specific work. In addition interesting problems for physics and mathematics arises out of such research. We hope this book will be an inspiring source of knowledge and ideas, stimulating further research in this exciting field. The promises and possible benefits of such efforts are manifold, they range from new transportation systems, intelligent cars to flexible assistants in factories and construction sites, over service robot which assist and support us in daily live, all the way to the possibility for efficient help for impaired and advances in prosthetics.

IntechOpen